This article has been accepted for publication in IEEE Transactions on Antennas and Propagation. This is the author's version which has not been fully edited and content may change prior to final publication. Citation information: DOI 10.1109/TAP.2023.3242110

Single-Layer Dual-/Tri-band SIW Filtenna Based on Multifunctional Cavity-Backed Slots

Zhirui Zheng, Daotong Li, *Senior Member, IEEE,* Xiaoheng Tan and Qiang Chen, *Senior Member, IEEE*

***Abstract*—Single-layer dual-/tri-band substrate integrated waveguide (SIW) filtenna based on multifunctional cavity-backed slots is proposed in this communication. The cavity-backed slots etched on the SIW cavity can be considered as radiators as well as resonators. When a pair of back-to-back open-loop slots embedded with a straight slot are etched on the SIW cavity, three resonant modes generated by slots combine with TE_{101} mode of the SIW cavity to form the superior dual-band filtering response. Moreover, four radiation nulls (RNs) located at both sides of two operational passbands are generated, resulting in the sharp roll-offs and deep stopband rejection. To further prove this design concept, a tri-band SIW filtenna is designed by utilizing two pairs of back-to-back open-loop slots embedded with a straight slot, six RNs are introduced in the stopbands, realizing the excellent tri-band filtering performance. The operating mechanism of the proposed antennas is numerically analyzed. Two prototype antennas are fabricated and tested to validation, the center frequencies of the dual-band filtenna are 4.56 and 5.7 GHz, and the tri-band filtenna are centered at 4.1, 4.82 and 5.62 GHz, showing good radiation characteristics in each passband. Compared with other designs, the proposed antennas exhibit the advantages of single-layer structure, small size and high selectivity, satisfying the requirements of 5G multi-frequency communication applications.**

***Index Terms*—Dual-band, tri-band, SIW, filtenna, cavity-backed slots.**

I. Introduction

Compared with single-band antennas [1]-[3], multi-band antennas not only hold the advantages of reducing the volume and cost of multi-frequency communication systems, but also increase the channel capacity under the crowded scenarios, such as stations and theaters. So multi-band antennas are widely investigated [4]. Meanwhile, filtennas are massively reported in recent years [5]-[8], due to their merits of decreasing the system size and reducing the insertion loss introduced in cascade with the filter. Therefore, the multi-band filtenna has the advantages of both the filtenna and the multi-band antenna, attracting much attention from scholars.

Recently, some multi-band filtennas in the form of microstrip are reported [9]-[13]. In [9]-[11], the dual-band microstrip filtennas are proposed by utilizing extra filtering circuits or networks, and the same technical form are also adopted by the tri-band microstrip filtennas [12]-[13]. However, because of the extra filtering circuits, larger occupied sizes, relatively complex structures or multi-layer substrates are inevitable, and the difficulty of processing and assembly also increases. Thus, the multi-band filtenna with the small size, simple and single-layer structure is highly desired.

Compared with the microstrip structures, substrate integrated waveguide (SIW) structures have the advantages of higher quality factor, higher power-handing capability and lower losses. Recently, SIW filtennas are widely investigated, but mostly focus on the single operating band [14]-[16]. To the best of the author's knowledge, there are few papers report SIW dual-band filtennas [17]-[19], and no tri-band SIW filtenna has been reported to date. The dual-band response with filtering performance can be realized by using a dual-mode cavity coupled to two orthogonally polarized slot-loaded SIW cavities [17]. However, the radiation nulls (RNs) need to be introduced in the stopband to further improve the frequency skirt selectivity and out-of-band suppression. In [18], through loading four metal-insulator-metal (MIM) capacitors and exciting two dual-mode rectangular cavity resonators, a dual-band SIW filtenna with improved stopband rejection is presented. However, the whole configuration becomes complex due to the MIM capacitors and two cascaded SIW cavities, and the processing difficulty is increased because of the stacked double-layer substrates. In [19], a single-layer dual-band half-mode SIW filtenna using high-order modes is proposed, which good filtering performance with three RNs is achieved. However, it suffers from a large size of 1.06 λ_0×1.02 λ_0×0.03 λ_0. From aforementioned designs, the poor filtering response without sufficient RNs, the complex multi-layer configuration and the large size are the three main problems of designing multi-band SIW filtennas. In addition, it should be ensured that the good radiation characteristics are maintained in each working band. Thus, it is very challenging to design SIW multi-band filtennas.

In this communication, single-layer dual-/tri-band SIW filtenna based on multifunctional cavity-backed slots is proposed for the first time. By using only one SIW cavity machined on the single-layer substrate, and etching one pair/two pairs of back–to-back open-loop slots embedded with a horizontal straight slot, the structure with small size is achieved. Three/five resonant modes of slots combine with TE_{101} mode of the SIW cavity to form the dual-/tri-band response. Each slot acts as a radiator as well as a resonator, showing the multifunctional property. Without any external filtering circuits, parasitic/stacked elements and complicated structure, four/six RNs are introduced in the stopband by source-load coupling and current cancellation, realizing the excellent dual-/tri-band filtering response with high selectivity and deep stopband rejection and reducing the complexity of double-/multi-layer configurations. The prototype antennas exhibited the small size only about 0.4 λ_0×0.5 λ_0×0.02 λ_0 are simulated, analyzed, fabricated and measured, good radiation characteristics are realized in each operating band, and the good agreement between simulated and measured results can be observed.

II. The Dual-Band SIW Filtenna

A. Antenna Configuration

Fig. 1 depicts the geometry of the proposed dual-band SIW filtenna named Proposed I, which consists of only three cavity-backed slots, four short pins and a pair of open stubs, realizing a simple structure. In details, a horizontal straight slot with width of W_1 is etched at the center of the SIW, and two open-loop slots with width of W_2/W_3 are located back-to-back on the upper and lower sides of the straight slot, respectively. Four short pins symmetrical about the SIW center are loaded to facilitate tuning the frequency of resonant modes. A couple of open stubs with length of L_{11} are loaded on the microstrip feedline to more easily adjust the antenna

This work was supported in part by the National Natural Science Foundation of China under Grant 61801059 and U20A200726, in part by the FY2021 JSPS Postdoctoral Fellowship for Research in Japan under Grant P21053, in part by the Grant-in-Aid for JSPS Research Fellow under Grant 21F21053. *(Corresponding Author: Xiaoheng Tan.)*

Zhirui Zheng, Daotong Li and Xiaoheng Tan are with School of Microelectronics and Communication Engineering, Chongqing University, Chongqing 400044, China (e-mail: zhengzhirui666@163.com; dli@cqu.edu.cn; txh@cqu.edu.cn).

Daotong Li and Qiang Chen are with the Department of Communications Engineering, Tohoku University, Sendai 980-8579, Japan (qiang.chen.a5@tohoku.ac.jp).

© 2023 IEEE. Personal use is permitted, but republication/redistribution requires IEEE permission. See https://www.ieee.org/publications/rights/index.html for more information.
Authorized licensed use limited to: TOHOKU UNIVERSITY. Downloaded on April 10,2023 at 05:45:36 UTC from IEEE Xplore. Restrictions apply.

This article has been accepted for publication in IEEE Transactions on Antennas and Propagation. This is the author's version which has not been fully edited and content may change prior to final publication. Citation information: DOI 10.1109/TAP.2023.3242110

impedance and enhance the upper stopband rejection. Additionally, a grounded coplanar waveguide (GCPW) transition structure is used between the microstrip feedline and SIW cavity. The overall structure of Proposed I is left-right symmetrical. The substrates used in this communication all are Rogers 4350 with relative permittivity of 3.48, loss tangent of 0.004 and thickness of 1.524 mm.

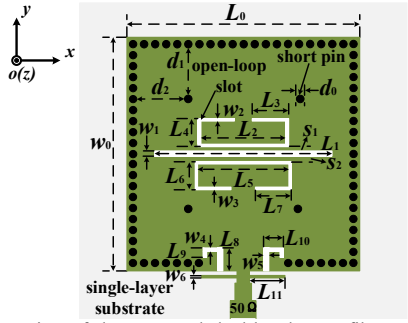

Fig. 1. Configuration of the proposed dual-band SIW filtenna (Proposed I) (L_0=29, L_1=22.1, L_2=9.4, L_3=4.2, L_4=3.3, L_5=9.6, L_6=3, L_7=4.2, L_8=3, L_9=1.4, L_{10}=2.2, L_{11}=4.86, w_0=30, w_1=0.45, w_2=0.3, w_3=0.3, w_4=0.4, w_5=0.7, w_6=0.32, d_0=0.5, d_1=6.67, d_2=6.67, s_1=0.29, s_2=0.4, unit: mm).

B. The Dual-Band Filtering Response

In order to get a deep insight into the operating mechanism of Proposed I, four reference antennas named Ant. I - IV and Proposed I are simulated and analyzed. Their structures and simulated results are presented in Fig. 2. In Fig. 2(a) and (c), two RNs and resonant modes f_1 and f_2 are generated by the initial structure Ant. I. However, the passband is not formed. Through loading four short pins on Ant. II, the passband with a RN on both sides is formed at higher frequencies. Because the electric field can be redistributed to influence the frequency by loading short pins. From the results of Ant. II, Ant. III and Ant. IV, it can be found that each open-loop slot (OLS_1 or OLS_2) introduces an RN and a resonant mode (f_3 or f_4). In addition, by comparing the results of Ant. IV and Proposed I in Fig. 2(b) and (d), it can be concluded that the impedance matching and the suppression of the upper stopband can be improved by loading a pair of open stubs on the microstrip feedline. As a result, the excellent dual-band filtering response with four RNs is achieved by Proposed I. To better distinguish, the four radiation nulls are labeled as RN_1-RN_4, as shown in Fig. 2(d).

The electric field (E-field) distributions at f_1, f_2, f_3 and f_4 are given in Fig. 3. At f_1, f_3 and f_4, the E-filed is mainly concentrated near the straight slot, OLS_1 and OLS_2, respectively, while the E-filed at f_2 mainly focuses on the center of the SIW cavity. It reveals that f_1, f_3 and f_4 are resonant modes of corresponding cavity-backed slots, and f_2 is TE_{101} mode of the SIW. The operating frequencies of cavity-backed slots and TE_{101} mode can be evaluated using formulas (1) and (2), respectively [2], [18]

$$f = \frac{c_0}{l \cdot \sqrt{2(\varepsilon_r + 1)}} \tag{1}$$

$$f_{TE101} = \frac{c_0}{2\sqrt{\varepsilon_r}} \sqrt{\left(\frac{1}{a}\right)^2 + \left(\frac{1}{b}\right)^2} \tag{2}$$

where l denotes the total length of the slot, c_0 is the light speed in vacuum, ε_r is relative permittivity of the substrate, and a and b denote the effective length and width of the SIW cavity, separately.

The effects of some key parameters on S_{11} are illustrated in Fig. 4. As can be seen, the frequency of each resonant mode can be adjusted independently, which has little impact on the frequencies of other modes. In addition, it can be found L_4 and L_6 have little influence on impedance matching of the upper passband, while d_1 has little effect on impedance matching of the lower passband.

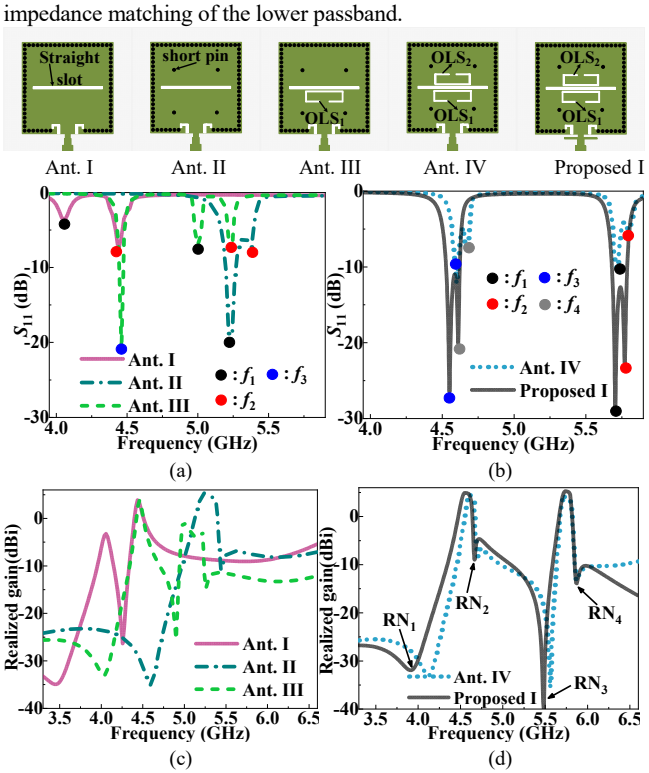

Fig. 2. Evolution of Proposed I. S_{11} of (a) Ant. I-Ant. III and (b) Ant. IV and Proposed I. Realized Gain of (c) Ant. I-Ant. III and (d) Ant. IV and Proposed I.

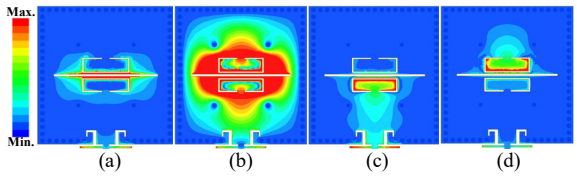

Fig. 3. E-field distributions at (a) f_1, (b) f_2, (c) f_3 and (d) f_4.

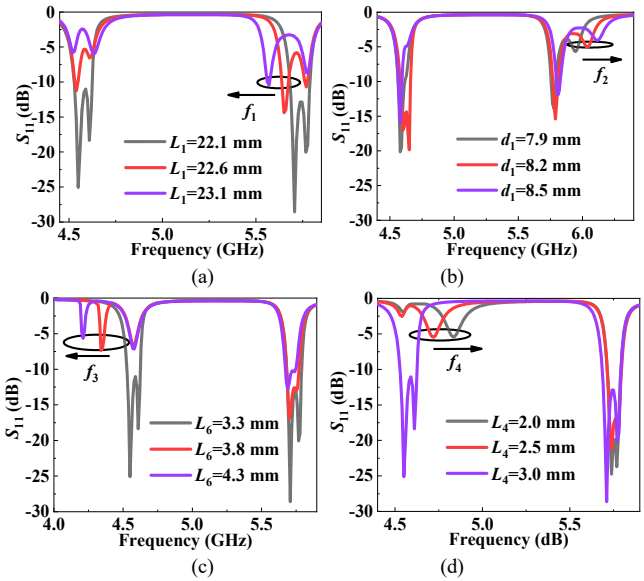

Fig. 4. Effects of (a) L_1, (b) d_1, (c) L_4 and (d) L_6 on S_{11}.

C. Coupling Topology and Coupling Matrix

© 2023 IEEE. Personal use is permitted, but republication/redistribution requires IEEE permission. See https://www.ieee.org/publications/rights/index.html for more information.
Authorized licensed use limited to: TOHOKU UNIVERSITY. Downloaded on April 10,2023 at 05:45:36 UTC from IEEE Xplore. Restrictions apply.

This article has been accepted for publication in IEEE Transactions on Antennas and Propagation. This is the author's version which has not been fully edited and content may change prior to final publication. Citation information: DOI 10.1109/TAP.2023.3242110

The coupling topology of Proposed I can be established as shown in Fig. 5, where S and L represent the source and load, separately, and the black nodes denote the resonators. Form source to load, multiple coupling paths can be observed. In the upper passband, the signal can be transmitted in the following coupling paths: S-f_1-L, S-f_1-f_2-L, S-f_2-L and S-f_2-f_1-L, while f_3 and f_4 are the spurious modes [18]. In the same principle, in the lower passband, coupling paths of the signal are: S-f_3-L, S-f_3-f_4-L, S-f_4-L and S-f_4-f_3-L, while f_1 and f_2 are the spurious modes. In addition, the source-load coupling is introduced by radiation leakage from the microstrip feedline and the GCPW transition structure [20], which is detailed in subsection D.

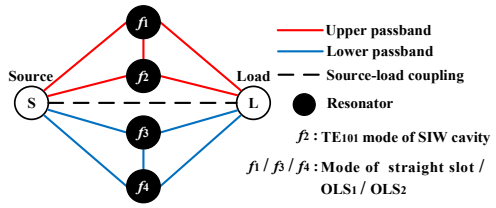

Fig. 5. The coupling topology of Proposed I.

Based on the coupling topology presented in Fig. 5, in the point of view of the filter design, the slots and TE_{101} mode can be treated as coupled resonators. The two operational passbands with quasi-elliptic function response can be obtained by coupled-resonator theory [18]. Thus, the coupling coefficients K_{ij} can be extracted from the simulated scattering parameters of two resonators and calculated by [21]

$$K_{ij} = \frac{f_j^2 - f_i^2}{f_j^2 + f_i^2} \tag{3}$$

where f_i and f_j (i=1, 3; j=2, 4; j-i=1) represent the resonant frequencies of resonators, which can be obtained from the S-parameters of two resonators with weakly coupled excitation by the external feed port. From subsection B, f_i and f_j can be adjusted independently to affect the coupling of two modes as a way to achieve the desired K_{ij}. The external quality factor Q_{ext} is mainly dominated by the GCPW transition structure, which can be adjusted by the insertion length and width of the GCPW coupling slots. Q_{ext} can be expressed as [21]

$$Q_{ext} = \frac{2\pi\tau f_0}{4} \tag{4}$$

where f_0 denotes the resonant frequency of the passband, and τ is the group delay of S_{11} at f_0. The desired coupling coefficients and external quality factors for the two operational passbands in this design are $K^{(I)}_{12}$=0.0167, $K^{(I)}_{34}$=0.0109, $Q^{(I)}_{e1}$=502.8 and $Q^{(I)}_{e2}$=450.3. Furthermore, the reference coupling matrix is guided and synthesized by the design method of bandpass filter [21]. The reference coupling matrix can be given as

$$M_1 = \begin{bmatrix} 0 & 0.24 & -0.14 & -0.13 & 0.18 & -0.05 \\ 0.24 & 0.97 & 0.64 & 0 & 0 & 0.24 \\ -0.14 & 0.64 & -0.77 & 0 & 0 & 0.14 \\ -0.13 & 0 & 0 & 0.80 & 0.62 & 0.13 \\ 0.18 & 0 & 0 & 0.62 & -0.62 & 0.18 \\ -0.05 & 0.24 & 0.14 & 0.13 & 0.18 & 0 \end{bmatrix} \tag{5}$$

D. Mechanism of Radiation Nulls

It can be clearly seen that a total of four RNs are introduced on both sides of the two operating passbands, which is depicted in Fig. 2(d). To reveal the forming mechanism of four RNs, the surface current distributions on the top layer at nulls are illustrated in Fig 6. At RN_1, currents mainly focus on the feed end and around OLS_1, and the current near the back side of OLS_1 is opposite with that at the feed end, as shown by arrows in Fig. 6(a). The microstrip feedline and GCPW transition structure generate the spurious radiation which is directly transmitted into the air acted as the load [20]. Thus, the spurious radiation directly couples to the load to generate source-load coupling, and can be cancelled out at the broadside direction by the out-of-phase radiation produced by OLS_1 with inverted currents, resulting in the generation of RN_1 [20]. Note that only Fig. 6(a) satisfies the conditions: (1) the current is mainly concentrated at the feed end and around the open-loop slot. (2) The current near the back side of the open-loop slot is 180° out-of-phase with that at the feed end. Therefore, different from reference [20], here only RN_1 is introduced by source-load coupling. Fig. 7 gives the comparison of Proposed I using microstrip feed and coaxial feed, further demonstrating that RN_1 is introduced by source-load coupling. As for the other three RNs, strong surface currents in red are primarily focused on the inside or outside of the cavity-backed slots, and they have equal magnitude but flow in opposite directions, as indicated by the arrows in Fig. 6(b), (c) and (d), respectively. Thus, the currents are cancelled out by each other to generate RN_2, RN_3 and RN_4 [14].

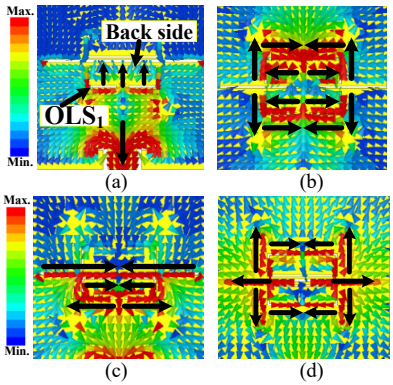

Fig. 6. Surface current distributions on top layer at the frequencies of (a) RN_1, (b) RN_2, (c) RN_3 and (d) RN_4.

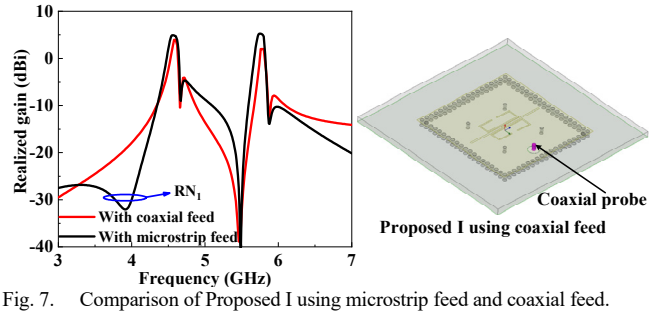

Fig. 7. Comparison of Proposed I using microstrip feed and coaxial feed.

E. Simulated and Measured Results

To validate the performance, the prototype of Proposed I is fabricated and tested. The simulated and measured S_{11} and realized gain are given in Fig. 8, and the antenna efficiency about 0.8 is shown in Fig. 9. The two measured passbands are located at 4.56 and 5.7 GHz, respectively, and the -10 dB impedance bandwidths are from 4.5 to 4.62 GHz and 5.66 to 5.76 GHz, separately. The tested average gain in both passbands are about 4.8 dBi, and the maximum measured gains are 4.87 and 5.07 dBi, respectively. Moreover, four notable RNs are generated in the stopband at 3.8, 4.65, 5.46 and 5.85 GHz, respectively, enhancing the sideband selectivity and stopband suppression greatly. The simulated and measured radiation patterns at 4.56 and 5.7 GHz are presented in Fig. 10. The good radiation characteristics in the dual-

© 2023 IEEE. Personal use is permitted, but republication/redistribution requires IEEE permission. See https://www.ieee.org/publications/rights/index.html for more information.
Authorized licensed use limited to: TOHOKU UNIVERSITY. Downloaded on April 10,2023 at 05:45:36 UTC from IEEE Xplore. Restrictions apply.

This article has been accepted for publication in IEEE Transactions on Antennas and Propagation. This is the author's version which has not been fully edited and content may change prior to final publication. Citation information: DOI 10.1109/TAP.2023.3242110

band can be observed. It can be seen that the E-plane and H-plane radiation patterns of two operating bands are relatively symmetrical and uniform. Moreover, the co-polarized fields of both E-plane and H-plane measured in the broadside direction are at least 18 dB stronger than their cross-polarized ones. In general, all aforementioned measured results agree well with their corresponding simulated values.

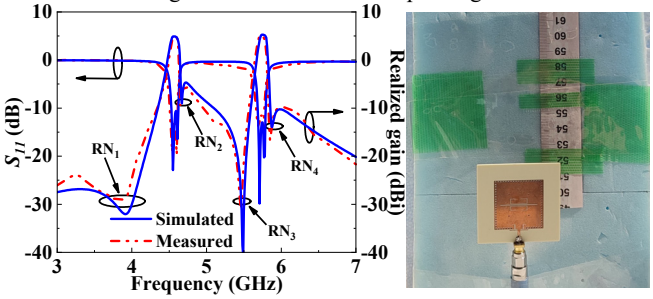

Fig. 8. Simulated and measured results and the fabricated antenna.

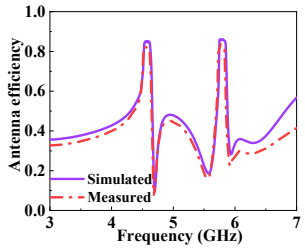

Fig. 9. Simulated and measured antenna efficiency.

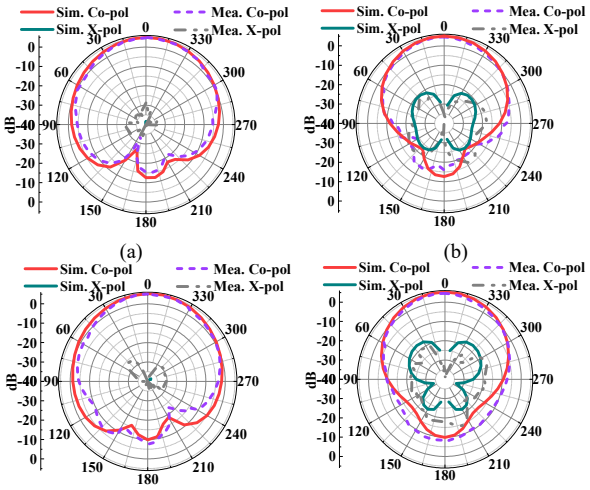

Fig. 10. Radiation patterns. (a) E-plane and (b) H-plane at 4.56 GHz. (c) E-plane and (d) H-plane at 5.7 GHz.

III. The Tri-Band SIW Filtenna

A. Antenna Configuration

Based on Proposed I, OLS_1 and OLS_2 are moved to the left side of the SIW, the newly added back-to-back open-loop slots OLS_3 and OLS_4 are etched on the right side of the SIW, and another couple of matching branches with length of L_{t18} are loaded on the feedline. Besides, four short pins are divided into left and right pairs to more flexibly adjust frequencies of modes. Thus, the proposed tri-band SIW filtenna named Proposed II is established as shown in Fig. 11.

B. The Tri-Band Filtering Response

The evolution of Proposed II and their simulated results are presented in Fig. 12. Although OLS_1 and OLS_2 are moved to the left side of the SIW, the dual-band filtering response with four RNs is still retained by Ant. 1. Moreover, it can be observed that both OLS_3 and OLS_4 introduce a resonant mode (f_5, f_6) and an RN (rn_5, rn_6). Thus, the tri-band filtering response with six RNs (rn_1-rn_6) is realized by Proposed II. Since proposed II has the same operating principle with Proposed I, here, only the E-filed distributions and parameter control of f_5 and f_6 are given. It proves that f_5 and f_6 are resonant modes of OLS_3 and OLS_4, respectively, which can be controlled independently and have little impact on the impedance matching of the lower and middle passbands, as shown in Figs. 12 and 13.

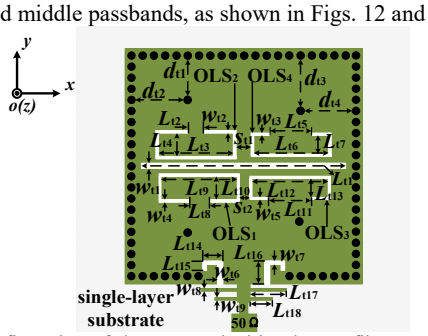

Fig. 11. Configuration of the proposed tri-band SIW filtenna (Proposed II) (L_{t1}=25.58, L_{t2}=1.6, L_{t3}=9.38, L_{t4}=3.68, L_{t5}=5.4, L_{t6}=9.3, L_{t7}=2.8, L_{t8}=1.64, L_{t9}=9.3, L_{t10}=3.3, L_{t11}=5.4, L_{t12}=9.2, L_{t13}=2.7, L_{t14}=2.9, L_{t15}=1.4, L_{t16}=3.4, L_{t17}=4.51, L_{t18}=3.17, w_{t1}=0.75, w_{t2}=0.31, w_{t3}=0.35, w_{t4}=0.35, w_{t5}=0.4, w_{t6}=0.85, w_{t7}=0.4, d_{t1}=3.97, d_{t2}=6.5, d_{t3}=4.77, d_{t4}=6.54, s_{t1}=1.4, s_{t2}=0.75, unit: mm).

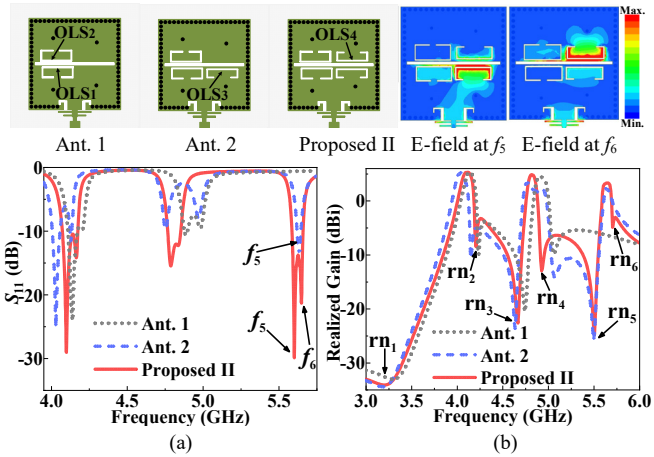

Fig. 12. Evolution of Proposed II and E-field at f_5 and f_6. (a) S_{11}. (b) Gain.

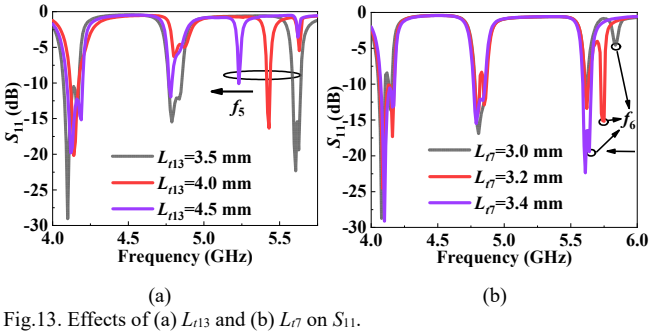

Fig.13. Effects of (a) L_{t13} and (b) L_{t7} on S_{11}.

C. Analysis of Proposed II

It is easy to conclude that Proposed II has the same mechanism with Proposed I. Therefore, in the point of view of filter design, TE_{101} mode, OLS_1, OLS_2, OLS_3 and OLS_4 all function as resonators, and the coupling topology of Proposed II can be established as

© 2023 IEEE. Personal use is permitted, but republication/redistribution requires IEEE permission. See https://www.ieee.org/publications/rights/index.html for more information.
Authorized licensed use limited to: TOHOKU UNIVERSITY. Downloaded on April 10,2023 at 05:45:36 UTC from IEEE Xplore. Restrictions apply.

This article has been accepted for publication in IEEE Transactions on Antennas and Propagation. This is the author's version which has not been fully edited and content may change prior to final publication. Citation information: DOI 10.1109/TAP.2023.3242110

shown in Fig. 14. The reference coupling matrix which is expressed by (6), is also synthesized by the coupled-resonator theory of filter design. Furthermore, the coupling coefficients and external quality factors still are evaluated by formula (3) and (4), and the calculated values of the three operational passbands are $K^{(II)}_{12}$=0.004, $K^{(II)}_{34}$=0.0083, $K^{(II)}_{56}$=0.0071, $Q^{(II)}_{e1}$=90.01, $Q^{(II)}_{e2}$=100.45 and $Q^{(II)}_{e3}$=80.87, respectively. To reveal the generation mechanism of six RNs, the surface current distributions at nulls are shown in Fig. 15. Obviously, rn_1 is still generated by source-load coupling, and rn_2-rn_6 still are introduced by the current cancellation inside or outside cavity-backed slots, which is detailed in Subsection *D* of Section II.

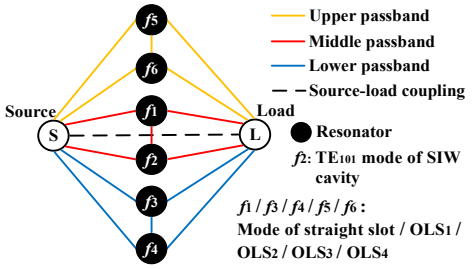

Fig. 14. The Coupling scheme of Proposed II.

$$M_2 = \begin{bmatrix} 0 & 0.35 & -0.08 & 0.16 & -0.08 & -0.14 & 0.2 & -0.1 \\ 0.35 & 1.02 & 0.16 & 0 & 0 & 0 & 0 & 0.35 \\ -0.08 & 0.16 & -1.01 & 0 & 0 & 0 & 0 & 0.08 \\ 0.16 & 0 & 0 & -0.93 & 0.05 & 0 & 0 & 0.16 \\ -0.08 & 0 & 0 & 0.05 & 0.84 & 0 & 0 & 0.08 \\ -0.14 & 0 & 0 & 0 & 0 & -0.08 & 0.02 & 0.14 \\ 0.2 & 0 & 0 & 0 & 0 & 0.02 & 0.06 & 0.2 \\ -0.1 & 0.35 & 0.08 & 0.16 & 0.08 & 0.14 & 0.2 & 0 \end{bmatrix} \quad (6)$$

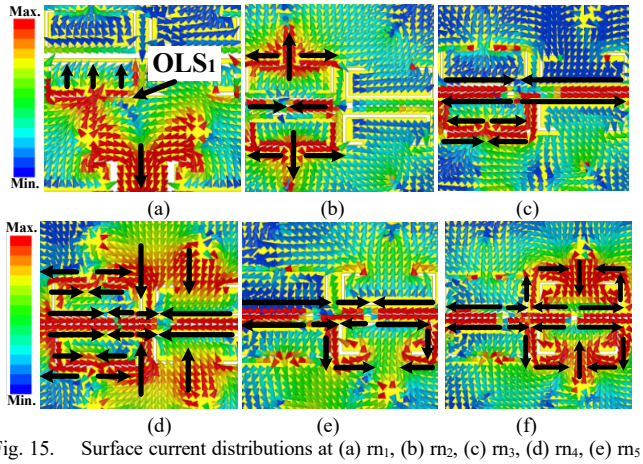

Fig. 15. Surface current distributions at (a) rn_1, (b) rn_2, (c) rn_3, (d) rn_4, (e) rn_5 and (f) rn_6.

D. Simulated and Measured Results

For demonstration, proposed II is fabricated and experimentally tested. The curves of S_{11} and realized gain are displayed in Fig. 16. The measured three operational passbands are centered at 4.1, 4.82 and 5.62 GHz, respectively. The maximum measured (simulated) realized gains are 5.05 (5.32), 4.58 (4.87) and 3.17 (3.33) dBi, respectively. Moreover, six RNs located at 3.21, 4.19, 4.67, 4.94, 5.5 and 5.69 GHz are introduced in the stopband, achieving the fast roll-offs at sidebands and the deep out-of-band suppression. In addition, at RNs of 3.21, 4.67 and 5.5 GHz, the stopband rejection level is over 20 dB, suppressing the interference signals greatly. Fig. 17 depicts the antenna efficiency. Fig. 18 presents the simulated and measured radiation patterns at the center frequencies of the three operating passbands. The good radiation characteristics can be obtained in all three passbands. The co-polarized levels in the broadside of E-plane and H-plane at the measured frequencies are at least 16 dB stronger than their corresponding cross-polarized levels. A good agreement can be observed between the tested results and the simulated ones.

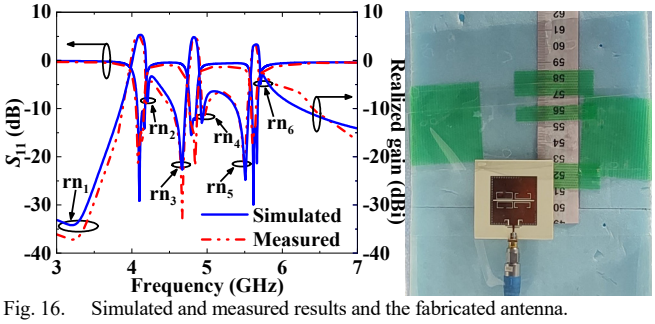

Fig. 16. Simulated and measured results and the fabricated antenna.

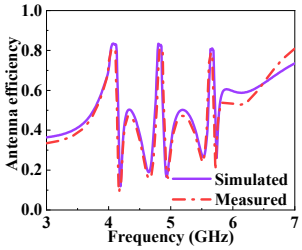

Fig. 17. Simulated and measured antenna efficiency.

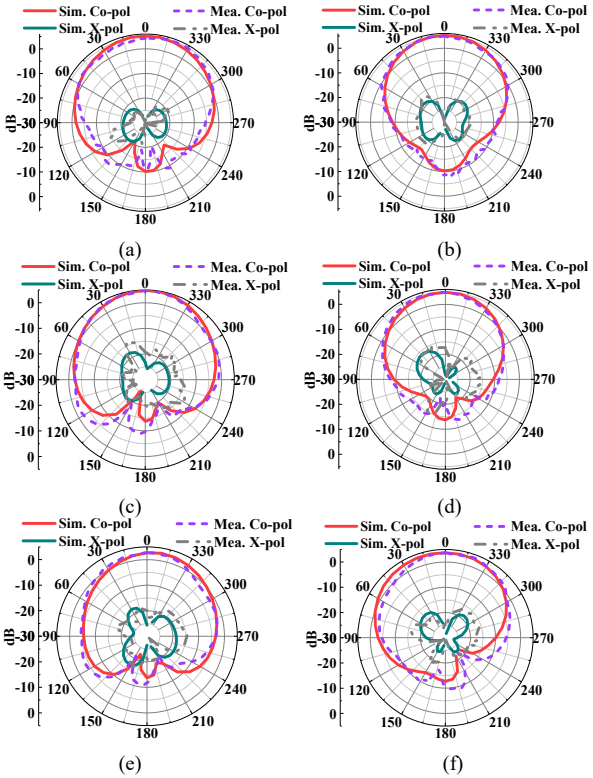

Fig. 18. Radiation patterns. (a) E-plane and (b) H-plane at 4.1 GHz. (c) E-plane and (d) H-plane at 4.82 GHz. (e) E-plane and (f) H-plane at 5.62 GHz.

IV. Comparisons

The comparisons of our proposed filtennas with some related filtennas recently reported are listed in Table I. In [5]-[7], cavity-backed slot filtennas based on metal waveguide cavity are proposed, exhibiting good filtering performance, high quality factor, high

© 2023 IEEE. Personal use is permitted, but republication/redistribution requires IEEE permission. See https://www.ieee.org/publications/rights/index.html for more information.
Authorized licensed use limited to: TOHOKU UNIVERSITY. Downloaded on April 10,2023 at 05:45:36 UTC from IEEE Xplore. Restrictions apply.

This article has been accepted for publication in IEEE Transactions on Antennas and Propagation. This is the author's version which has not been fully edited and content may change prior to final publication. Citation information: DOI 10.1109/TAP.2023.3242110

power-handing capability and low losses. However, only the single operating passband is realized, and the bulky volume, heavy weight and high cost are inevitable due to the metal waveguide structure that is not easy to integrate. Even though the dual-band filtenna in [9] has a relatively small size, it adopted double-layer substrate and only has two RNs in the stopband. In [10], [17]-[19], although the good dual-band filtering performance is realized, the number of RNs is still insufficient, showing relatively poor selectivity and suppression in the middle stopband. Moreover, these designs occupy a large size, especially for [17] and [19]. In [12], the tri-band filtering response is obtained by using microstrip structure, however, the poor roll-off rate is inevitable since there are only three RNs far from the passbands. In addition, double-layer substrates increase the complexity and cost of fabrication. Our proposed antennas not only exhibit dual-band and tri-band filtering response with four and six RNs, separately, realizing the sharp roll-off rate and deep stopband rejection level, but also feature the characteristics of single-layer substrate and small sizes of only 0.40 λ_0×0.53 λ_0×0.02 λ_0 and 0.40 λ_0×0.58 λ_0×0.02 λ_0, respectively.

TABLE I
COMPARISONS BETWEEN PROPOSED FILTENNAS AND RELATED FILTENNAS

Ref	NP	RN	Size (λ_0×λ_0×λ_0)	LS	SRL (dB)	Type
[5]	1	0	0.97×0.89×1.48	N.A.	N.A.	MWC
[6]	1	2	3.67×0.70×0.27	N.A.	17/13	MWC
[7]	1	2	0.72×0.63×1.55	N.A.	14/23	MWC
[9]	2	2	0.37×0.52×0.01	2	16.5/22.5	MS
[10]	2	3	0.96×0.96×0.01	1	20.5/17/23	MS
[12]	3	3	0.73×0.27×0.05	2	26.5/19/21	MS
[17]	2	2	1.29×1.29×0.01	1	25.5/21.5	SIW
[18]	2	3	0.76×0.73×0.04	2	37/36.5/20	SIW
[19]	2	3	1.06×1.02×0.03	1	15/35/24	SIW
Prop. I	**2**	**4**	**0.40×0.53×0.02**	**1**	**29.1/9.5/31.1/17**	**SIW**
Prop. II	**3**	**6**	**0.40×0.58×0.02**	**1**	**37.2/9.1/32.8/ 12.2/21.9/4.9**	**SIW**

NP represents number of passbands; RN is radiation null; LS denotes layers of substrates; SRL is sideband rejection level (determined by locations of radiation nulls); MWC represents metal waveguide cavity; MS denotes microstrip.

V. CONCLUSIONS

Single-layer dual-/tri-band SIW filtenna based on multifunctional cavity-backed slots is proposed in this communication. By etching one pair/two pairs of back-to-back open-loop slots embedded with a straight slot on the single SIW cavity, each slot acts as a radiator and a resonator, simultaneously. The resonance modes of the slots and TE_{101} mode of the SIW cavity are combined in pairs to form the dual-/tri-band filtering response. Four/six RNs are introduced in the stopband and are located at both sides of each passband, resulting in the sharp roll-off rate and deep stopband rejection. Moreover, good radiation characteristics are achieved in each operating band. The prototype antennas are fabricated and measured, the measured results agree well with corresponding simulated values. The proposed dual-band filtenna works at 4.56 and 5.7 GHz, the maximum measured realized gain are 4.87 and 5.07 dBi, respectively. The proposed tri-band filtenna operates at 4.1, 4.82 and 5.62 GHz, the maximum measured realized gain are 5.05, 4.58 and 3.17 dBi, separately. Both prototype antennas feature the single layer structures with small sizes of only 0.40 λ_0×0.53 λ_0 ×0.02 λ_0 and 0.40 λ_0×0.58 λ_0×0.02 λ_0, respectively, and meet the requirements of 5G multi-frequency communication applications.

REFERENCES

[1] W. Wu, K. -D. Xu, Q. Chen, T. Tanaka, M. Kozai and H. Minami, "A Wideband Reflectarray Based on Single-Layer Magneto-Electric Dipole Elements with 1-Bit Switching Mode," *IEEE Trans. Antennas Propag.*, vol. 70, no. 12, pp. 12346-12351, Dec. 2022.

[2] A. J. Farrall and P. R. Young, "Integrated waveguide slot antennas," *Electron. Lett.*, vol. 40, no. 16, pp. 974-975, 5 Aug. 2004.

[3] Daotong Li, Yaqing Yu, Ming-Chun Tang, Dajiang Li, Dongmei Mu, Mei Li, "Active, compact, wideband, receiving filtenna with power adaptation for space-limited wireless platforms," *Chin. J. Aeronaut.*, vol. 35, no. 8, pp. 7-11, 2022.

[4] T. Hong, Z. Zhao, W. Jiang, S. Xia, Y. Liu and S. Gong, "Dual-Band SIW Cavity-Backed Slot Array Using TM_{020} and TM_{120} Modes for 5G Applications," *IEEE Trans. Antennas Propag.*, vol. 67, no. 5, pp. 3490-3495, May 2019.

[5] Y. -M. Wu, S. -W. Wong, H. Wong and F. -C. Chen, "A Design of Bandwidth-Enhanced Cavity-Backed Slot Filtenna Using Resonance Windows," *IEEE Trans. Antennas Propag.*, vol. 67, no. 3, pp. 1926-1930, March 2019.

[6] W. Wang, "A Waveguide Slot Filtering Antenna With an Embedded Metamaterial Structure," *IEEE Trans. Antennas Propag.*, vol. 67, no. 5, pp. 2953-2960, May 2019.

[7] K. -R. Xiang, F. -C. Chen and Q. -X. Chu, "High Selectivity and High Gain X-Band Waveguide Filtering Antenna Based on Triple-Mode Resonator," *IEEE Trans. Antennas Propag.*, vol. 69, no. 10, pp. 6953-6958, Oct. 2021.

[8] W. Yang, M. Xun, W. Che, W. Feng, Y. Zhang and Q. Xue, "Novel Compact High-Gain Differential-Fed Dual-Polarized Filtering Patch Antenna," *IEEE Trans. Antennas Propag.*, vol. 67, no. 12, pp. 7261-7271, Dec. 2019.

[9] C.-Y. Hsieh, C.-H. Wu and T.-G. Ma, "A Compact Dual-Band Filtering Patch Antenna Using Step Impedance Resonators," *IEEE Antennas Wireless Propag. Lett.*, vol. 14, pp. 1056-1059, 2015.

[10] K. Dhwaj, L. J. Jiang and T. Itoh, "Dual-Band Filtering Antenna With Novel Transmission Zero Characteristics," *IEEE Antennas Wireless Propag. Lett.*, vol. 17, no. 12, pp. 2469-2473, Dec. 2018.

[11] C. X. Mao and Steven Gao, "Dual-Band Patch Antenna With Filtering Performance and Harmonic Suppression," *IEEE Trans. Antennas Propag.*, vol. 64, no. 9, pp. 4074-4077, Sept. 2016.

[12] J. Qian, F. Chen and Q. Chu, "A Novel Tri-Band Patch Antenna With Broadside Radiation and Its Application to Filtering Antenna," *IEEE Trans. Antennas Propag.*, vol. 66, no. 10, pp. 5580-5585, Oct. 2018.

[13] Y. Xie, F. Chen and J. Qian, "Design of Integrated Duplexing and Multi-Band Filtering Slot Antennas," *IEEE Access*, vol. 8, pp. 126119-126126, 2020.

[14] J.-Y. Yin, Tao-Long Bai and Jing-Ya Deng, "Wideband Single-Layer Substrate Integrated Waveguide Filtering Antenna With U-Shaped Slots," *IEEE Antennas Wireless Propag. Lett.*, vol. 20, no. 9, pp. 1726-1730, Sept. 2021.

[15] H.-Y. Xie, B. Wu, Y.-L. Wang, C. Fan, J.-Z. Chen and T. Su, "Wideband SIW Filtering Antenna With Controllable Radiation Nulls Using Dual-Mode Cavities," *IEEE Antennas Wireless Propag. Lett.*, vol. 20, no. 9, pp. 1799-1803, Sept. 2021.

[16] C. Wang, X. Wang, H. Liu, Z. Chen and Z. Han, "Substrate Integrated Waveguide Filtenna With Two Controllable Radiation Nulls," *IEEE Access*, vol. 8, pp. 120019-120024, 2020.

[17] K. Dhwaj, H. Tian and T. Itoh, "Low-Profile Dual-Band Filtering Antenna Using Common Planar Cavity," *IEEE Antennas Wireless Propag. Lett.*, vol. 17, no. 6, pp. 1081-1084, June 2018.

[18] D. Zhao, F. Lin, H. Sun and X. Y. Zhang, "A Miniaturized Dual-Band SIW Filtering Antenna With Improved Out-of-Band Suppression," *IEEE Trans. Antennas Propag.*, vol. 70, no. 1, pp. 126-134, Jan. 2022.

[19] L. Li, S. Wu, D. Pang, X. Zhang and Q. Wang, "A Fifth-Order Single-Layer Dual-Band Half-Mode SIW Filtering Antenna With a Multifunctional Single Slot," *IEEE Antennas Wireless Propag. Lett.*, vol. 20, no. 9, pp. 1676-1680, Sept. 2021.

[20] K. Dhwaj, J. M. Kovitz, H. Tian, L. J. Jiang and T. Itoh, "Half-Mode Cavity-Based Planar Filtering Antenna With Controllable Transmission Zeroes," *IEEE Antennas Wireless Propag. Lett.*, vol. 17, no. 5, pp. 833-836, May 2018.

[21] J. S. Hong and M. J. Lancaster, *Microstrip Filter for RF/Microwave Applications*. New York, NY, USA: Wiley, 2001.

© 2023 IEEE. Personal use is permitted, but republication/redistribution requires IEEE permission. See https://www.ieee.org/publications/rights/index.html for more information.
Authorized licensed use limited to: TOHOKU UNIVERSITY. Downloaded on April 10,2023 at 05:45:36 UTC from IEEE Xplore. Restrictions apply.